# CHARACTERIZING THE INFLUENCE OF PRINT PARAMETERS ON POROSITY AND RESULTING DENSITY

James Brackett[1], Dakota Cauthen[2], Justin Condon[2,3], Tyler Smith[2,3]
Nidia Gallego[3], Vlastamil Kunc[2,3], Chad Duty[2,3]

[1] Energy Science and Engineering, University of Tennessee – Knoxville, TN
[2] Mechanical, Aerospace, and Biomedical Engineering, University of Tennessee – Knoxville, TN
[3] Oak Ridge National Laboratory, TN

## Abstract

Extrusion deposition additive manufacturing produces parts with inherent porosity, which typically manifests as easily accessible voids between beads. This open porosity can also be accompanied by voids within the beads themselves, and both types can impact a part's desired performance. Porosity is influenced by a variety of factors, including infill percentage, layer height, nozzle diameter, print speed, and raster orientation. While their influence on mechanical properties and porosity have been studied previously, there has been minimal work connecting print parameters to porosity and subsequently to mechanical performance. This study investigates the relationships between print parameters, volumetric porosity, and mechanical performance. In addition, this study measures both open and closed porosity through use of a helium pycnometer rather than image analysis of a cross-section. Thus, this study will identify correlations between the volumetric density of parts and the resulting mechanical performance as a function of print parameters.

## Introduction

Extrusion deposition Additive Manufacturing (AM) techniques vary in extrusion process and materials, but one of the most common processes is Fused Filament Fabrication (FFF) of thermoplastic polymers. While not limited to small-scale, the technique is most often associated with desktop printers found in homes and labs across the nation. The popularity of commercial units is largely due to FFF's ease of use and affordability, but it still maintains important applications in modelling, prototyping, and small-batch production [1]. However, FFF does encounter issues with resolution and porosity, which the scale of the layer-based structure inherently introduces [2]. From a material standpoint, FFF is compatible with a wide range of thermoplastics, but one of the most popular choices is Acrylonitrile-Butadiene-Styrene (ABS). ABS material properties provide easy processing conditions for FFF while its price-point is lower than many engineering plastics, providing a useful middle-ground [3]. Thus, ABS is an ideal candidate for examining the FFF process and its inherent influences on the properties of printed structures.

There have been numerous investigations into the influence of environmental conditions, material characteristics, and printing parameters on the FFF process and the resulting properties of printed structures. To demonstrate environmental dependence, Sun et al investigated the effects of variation in processing temperatures on the quality of bonding between adjacent rasters. Through measurement of neck formation and flexural loading, they demonstrated the

importance of controlling cooling to improve mechanical performance through increased raster bonding [4]. While ABS is one of the more popular choices for FFF systems, they are compatible with a variety of thermoplastics, each of which has its own distinct properties and suggested printing parameters. For example, PolyLactic Acid (PLA), another extremely common FFF material, can vary from one brand of PLA to the next. Wittbrodt and Pearce compared the tensile performance of five different colors of PLA at four different extruder temperatures, and they found that each color had a distinctly different performance with extruder temperature further altering tensile strength as a result of variation in crystallinity [5]. However, in a study of seven different thermoplastic filaments, it has been shown that the exhibited tensile strength is a direct product final mass as a function of the theoretical mass, regardless of material, which led the team to identify under-extrusion in the interior as the culprit for inconsistencies in tensile strength [6]. Even within a given set of environmental and material conditions, the chosen print parameters still further influence FFF printing. The number of layers within a part, for instance, was found to affect the mechanical performance such that observed moduli and strength values steadily increased until reaching a substantial number of layers (12 at 0.2 mm layer height) [7]. Similarly, Wu et al found a "sweet spot" in layer height experiments where a layer height of 0.3 mm significantly outperformed both a 0.2 mm and a 0.4 mm layer height [8]. In a further exploration of Letcher's work, Rankouhi et al demonstrated an improved performance at smaller layer heights and through optical microscopy, attributed the improvement to the reduction in the "air-gap to material ratio" that was seen at a 0.2 mm height vs the 0.4 mm height, meaning there was more material in the mesostructure of the 0.2 mm samples [9]. Each of these studies also incorporated a varying raster angle in their experimental process; unidirectionally, 0° raster angle outperformed a 45° and 90° orientation while Wu found the best performance in an alternating 0°/90° orientation compared to a 30°/-60° and 45°/-45° orientation [7-9]. An analytical study of more possible raster orientations found agreement with these results, showing a continual decrease in Ultimate Tensile Strength (UTS) with increasing raster orientation angle [10]. Another parameter of interest is the infill percentage. Alvarez et al studied the effectiveness of printing from 0% to 100% infills and found minimal performance improvements for infills from 50% - 98%, after which there was as significant jump [11]. Hossain et al investigated multiple build parameters (build orientation, raster orientation, raster width, contour width, and air gap between rasters), and while all were found to have significant impacts on the UTS, they also demonstrated that a negative air gap could be used to eliminate space between rasters for a nearly defect-free part with dramatically improved UTS [12]. Ning et al similarly took a multi-parameter approach, demonstrating the same orientation effect as Wu [8], similar increases in UTS and modulus at shorter layer heights [8, 9], and maximum tensile performance at intermediate nozzle temperatures and infill speeds [13]. In another investigation into print parameters, Balani et al examined the influence of nozzle diameter, layer height, feed rate, and material rheology on material characteristics in an FDM's liquefier, which found that controlling for a lower viscosity improves print bonding quality [14]. Bead shape as a result of print parameters is equally important, and Serdeczny et al developed an improved numerical model for predicting the cross-sectional shape of an extruded bead that outperformed other techniques in common print parameter ranges despite excluding viscoelastic effects and temperature-dependent material properties [15]. While not a comprehensive list, there are obviously numerous parameters that can influence an FFF printed part and extensive study has been devoted to understanding each one's contribution.

Although there have been numerous investigations into the effects of layer height, infill percentage, and porosity on mechanical properties, they generally consider only one or two of the three. In this work, we seek to examine all three simultaneous and investigate how each are connected. To that end, we examine the influence of layer height and infill percentage on the porosity of a printed sample before moving forward to consider the influence of the print parameters and resulting porosity on the UTS and elastic modulus of tensile specimens. This approach is intended to capture the effects of each parameter separately and the effect of their combined presence.

## Experimental

Purple Matter Hacker Build Series ABS filament [16] was used to print all samples on a MakerGear M2. The filament was received sealed and dried before being immediately used, and it was maintained in a dry environment during the printing process.

### Print Parameters

All print parameters other than those being studied were held constant. The extrusion multiplier was set to 1.0, filament diameter of 1.75 mm, infill angle of $\pm45°$, bed temperature of 80°C, nozzle temperature of 235°C, print speed of 60 mm/s, solid infill speed of 20 mm/s, nozzle diameter 0.35 mm, and 0 perimeters. The parameters chosen for study were the infill percentage and layer height. Additionally, the chosen layer heights were obtained as ratios of nozzle diameter to enable a more direct comparison to other nozzle sizes. Table 1 shows the resulting layer heights and infill percentages used, each of which was printed with all four settings from the opposite row for a total of 16 parameter pairs.

**Table 1:** Parameters Under Investigation

| Layer Heights (mm) | 0.155 | 0.175 | 0.200 | 0.235 |
|---|---|---|---|---|
| Infill Percentages | 85% | 90% | 95% | 100% |

### Print and Sample Geometry

For this investigation, each parameter set was printed as a flat, rectangular plate. This method was chosen to avoid the stress concentrations brought about by geometric discontinuities in the radial regions that are associated with printing dogbone tensile samples directly. Tensile samples were then machined from the plates using waterjet cutting in an orientation that preserved the $\pm45°$ infill structure. Machining dimensions were taken from ASTM D638-14 Type V specifications [17]. The plates were 111.125 mm by 88.9 mm (4.375 in by 3.5 in) to allow for eight dogbones to be extracted and ensure statistical relevance. Samples that experienced damage or delamination, about one per plate, at any point were discarded. Furthermore, the chosen print parameters produced three plates that failed during printing due to

bed delamination: the 100% infill with 0.155 mm and 0.175 mm layer height and the 95% infill with 0.155 mm layer height. Figure 1 shows the process from printed plate to extracted samples.
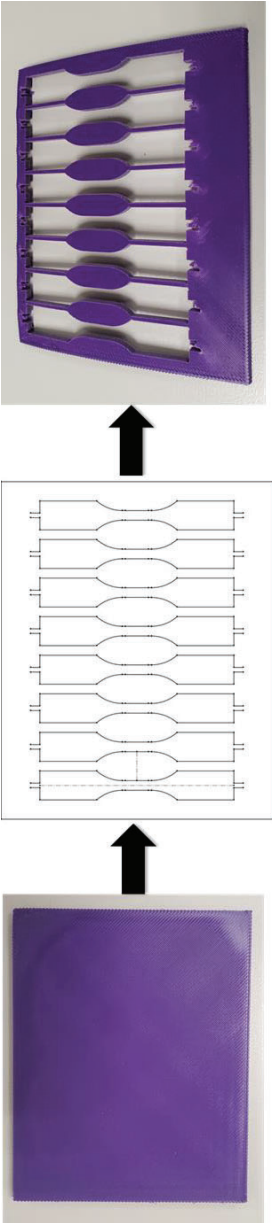


**Figure 1:** The printed plate, the schematic of the waterjet cutting pathway, and the plate with tensile bars extracted.

## Density and Porosity Calculations

Multiple methods are available for determination of porosity or density of an object. The most common is simply to divide mass by the volume of the object, but obtaining the exact volume of a complex object is difficult. Another technique is Gas pycnometry, which utilizes an inert gas to compare the volumes of two chambers. For this investigation, helium pycnometry was chosen for its ease of use, ability to infiltrate open porosity, and accuracy. This was supported by indirect volume calculation for traditional density measurements, wherein the xy cross-sectional area was used for convenience given the large number of samples.

Helium pycnometry was conducted with a Quantachrome Instruments' Ultrapycnometer 1000, MUPY-15 to find the apparent density of the filament prior to printing and several samples representative of four printed plates. With this method, a chamber containing the sample in question is compared to a reference chamber. Both chambers are of a known, similar volume, so the volumetric displacement of the sample can be measured by comparing the pressures in the chambers. Given helium's small molecular size, the gas infiltrates any open porosity, which results in the technique's ability to obtain a density measurement that disregards open porosity.

A secondary method was used to find the volumetric density of each individual dogbone that included the open porosity inherent in its structure. The xy cross-sectional area, $A_{xy}$, was taken from the machining file and compared to physical measurements to check with accuracy. Easily measured dimensions were compared to the file and found accurate enough to proceed with using the machining file's area estimate. From there, each dogbone's thickness was measured at five locations across its length using hand-held calipers to obtain an average thickness, $t$. Finally, each sample's mass, $m$, was measured to a 1 mg accuracy. Using $t$, $m$, and $A_{xy}$ as seen below, the density, $\rho_{print}$, of each sample was calculated.

$$\rho_{Print} = \frac{m}{t * A_{xy}}$$

To obtain a porosity measurement, the filament's apparent density returned by the helium pycnometry was treated as a maximum. The volumetric density of each Type V sample was then

divided by the filament density to find its approximate percent density, which was subtracted from 100 to find percent porosity in the printed samples.

**Tensile Testing**

Tensile testing of all Type 5 dogbones was conducted on an MTS Criterion Series, Model 45 with a 10kN load cell to accommodate the low force required for failure. A testing rate of 1mm/min was used for a nominal strain rate of 0.1 mm/(mm*min). Extension was measured using an MTS LX 500 Laser Extensometer. Samples that fractured outside of the gage length were not included in data analysis.

<u>**Results and Discussion**</u>

**Apparent and Volumetric Density Measurements**

Figure 2 shows the apparent density measured via helium pycnometry. The measured density for the filament is greater than that of the printed samples, but even with the distinct difference, the 0.155 mm layer height's apparent density showed a less than 2% difference. Given that all other plates fall in between the two, the printing process appears to introduce minute amounts of closed porosity into the filament strands. This is likely a result of both standard deviation in the measurement process and possibly a small amount of air infiltration within the melt inside the extruder.
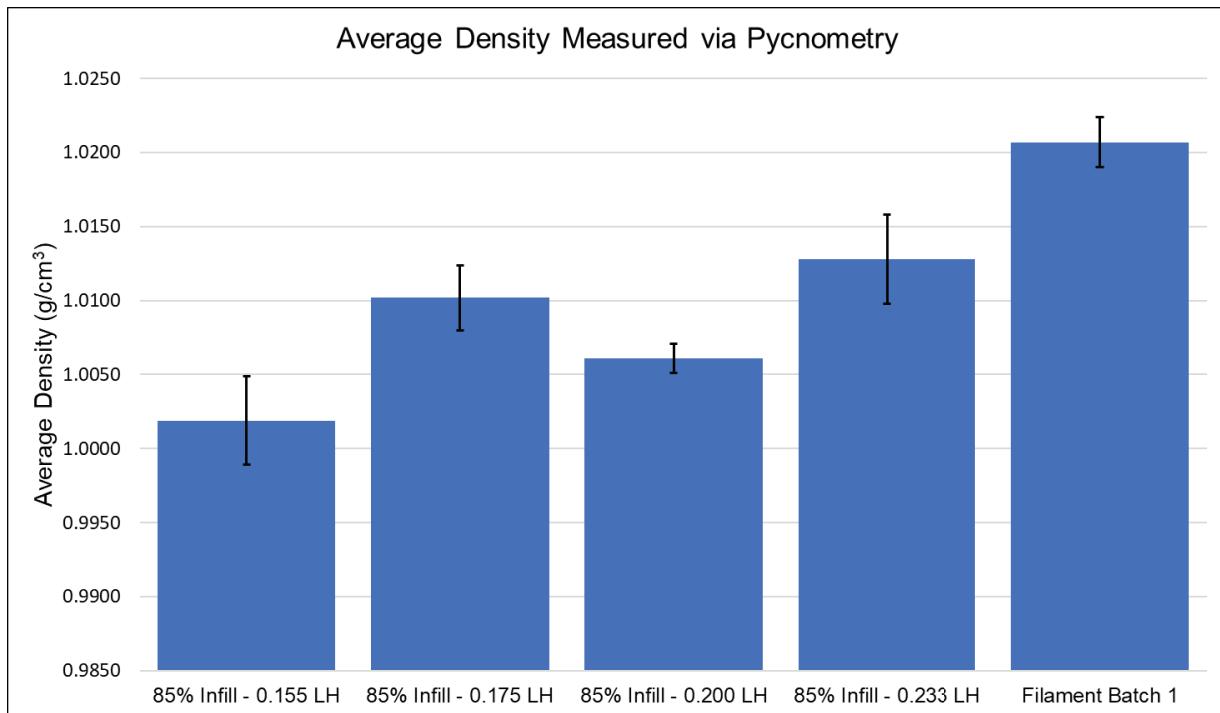


**Figure 2:** Apparent densities of four representative samples from printed plates and the filament used to print them.

Since FFF processes inherently produce structural porosity within a part, it was expected that helium pycnometry measurements would show a minimal difference and essentially measure the density of the beads within the piece. While Figure 2 supports this, Figure 3 confirms that the "true" density of the printed dogbones was significantly lower than those obtained through pycnometry. For example, at the lowest point, the print density was only 82% of filament's apparent density. Furthermore, the density of samples increased linearly with infill percentage. Figure 4 provides a closer picture of layer height's more nuanced influence on density. Although the difference was minimal, 85% and 90% infills exhibited a gradual decrease in density with increasing layer height: a 3% decrease in the 8% infill set and a 5% decrease for 90% infill. This effect was not seen for the 95% and 100% infills, for they exhibited no correlation between layer height and density.
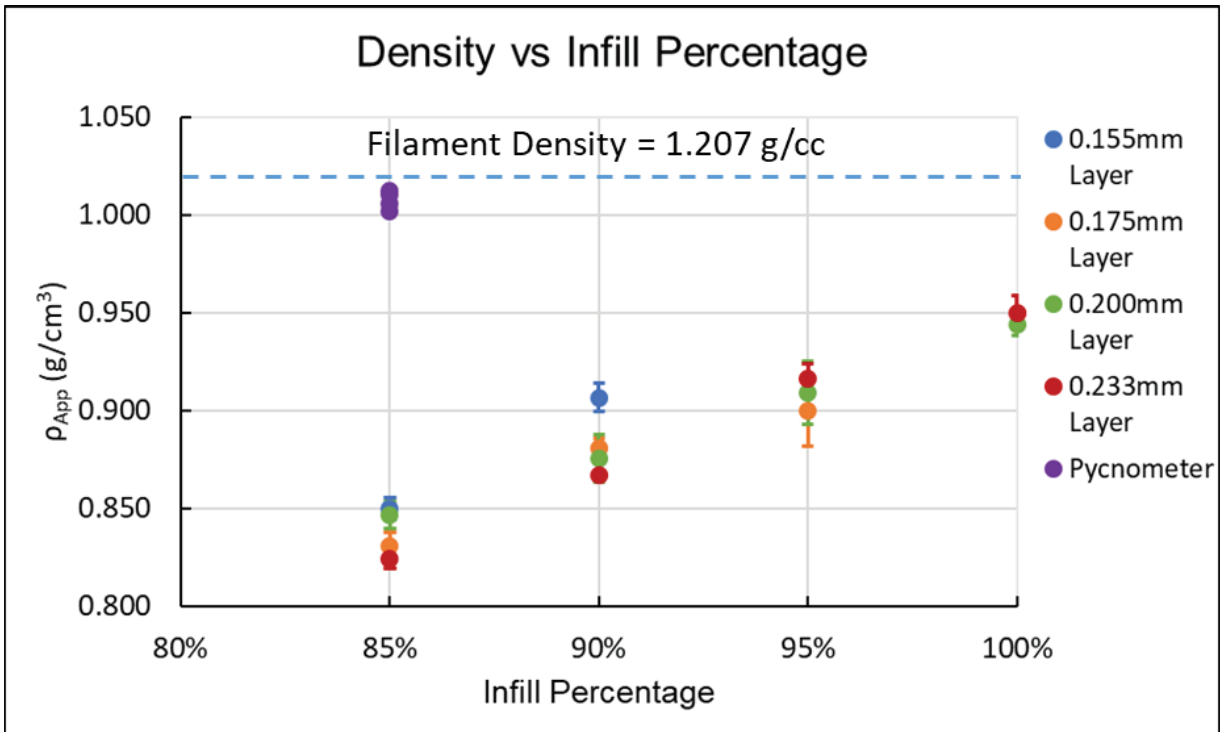


**Figure 3:** Comparison of the physically measured densities to the apparent density measured by helium pycnometry. The densities of printed samples are grouped by layer height.
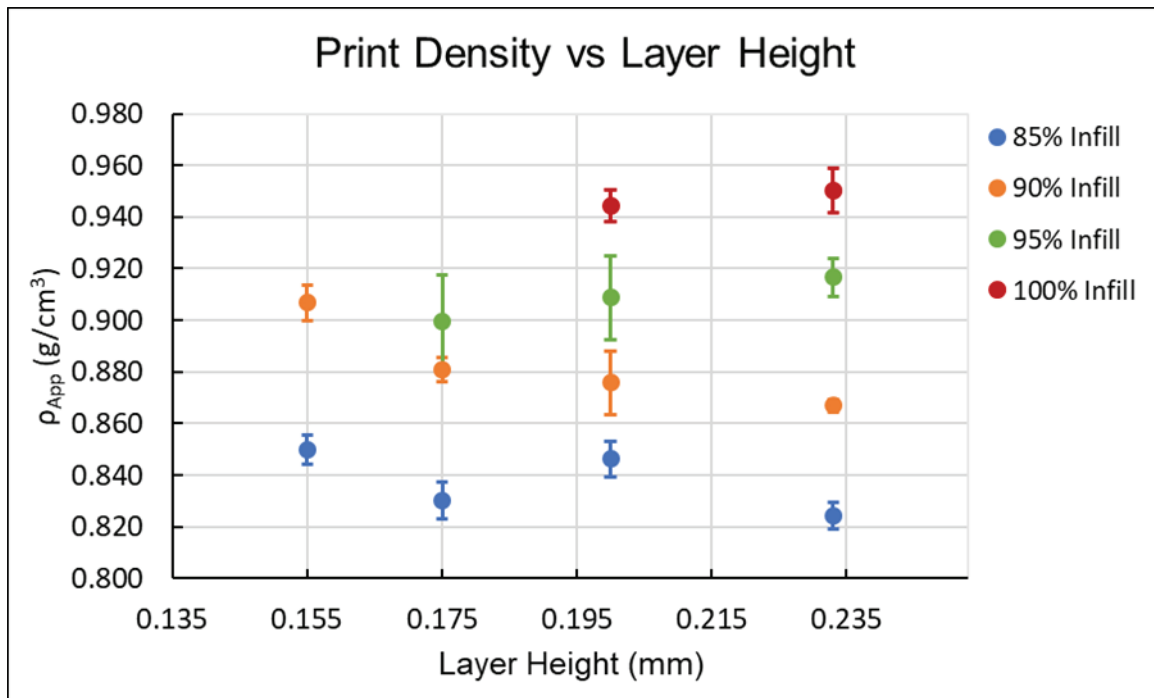
**Figure 4:** Print density without helium pycnometry's apparent density measurements. Measurements were grouped by infill percentage to examine the influence of layer height.

**Young's Modulus as a Function of Print Parameters**

Before comparing mechanical properties directly to density, a baseline of density above and mechanical performance below was established relative to print parameters. Figure 5 exhibits a clear trend of increasing elastic modulus with increasing infill percentage, up to a maximum of 216% from the 0.233 mm layer height at 85% infill to the 0.233 mm layer height at 100% infill. However, it does experience a plateau effect moving from 95% to 100% infills. Once again, Figure 6 considers layer height's influence on the modulus and yields two separate trends. As before, the 85% and 90% infills experience a decrease in modulus with increasing layer height – up to 47% and 40% respectively. However, no substantial difference is observed between layer heights at 9% and 100% infills. Figure 5 indicates that increasing infill past 95% yields diminishing returns on modulus improvement while Figure 6 shows that layer height remains important in determining the modulus until a threshold between 90% and 95% infill.
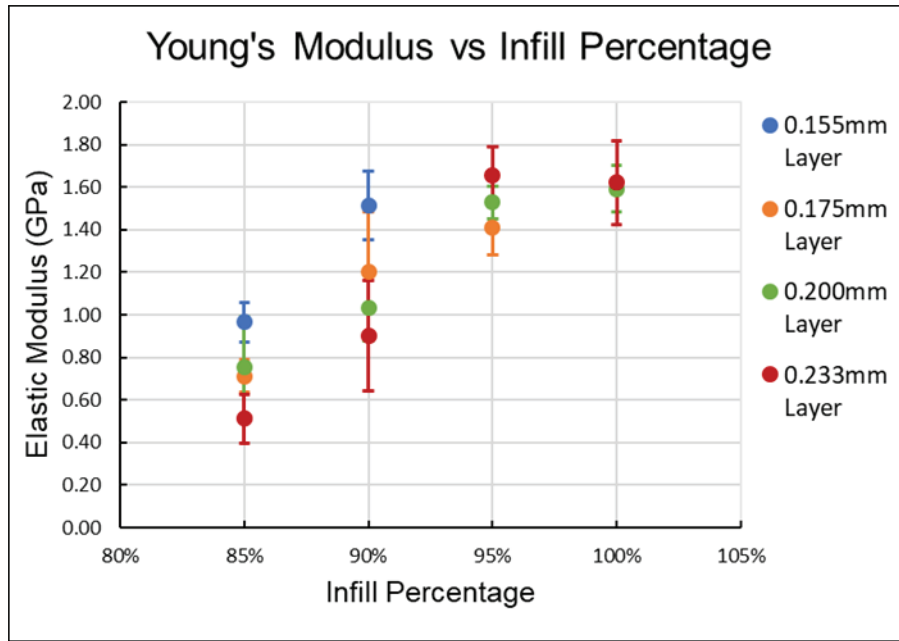
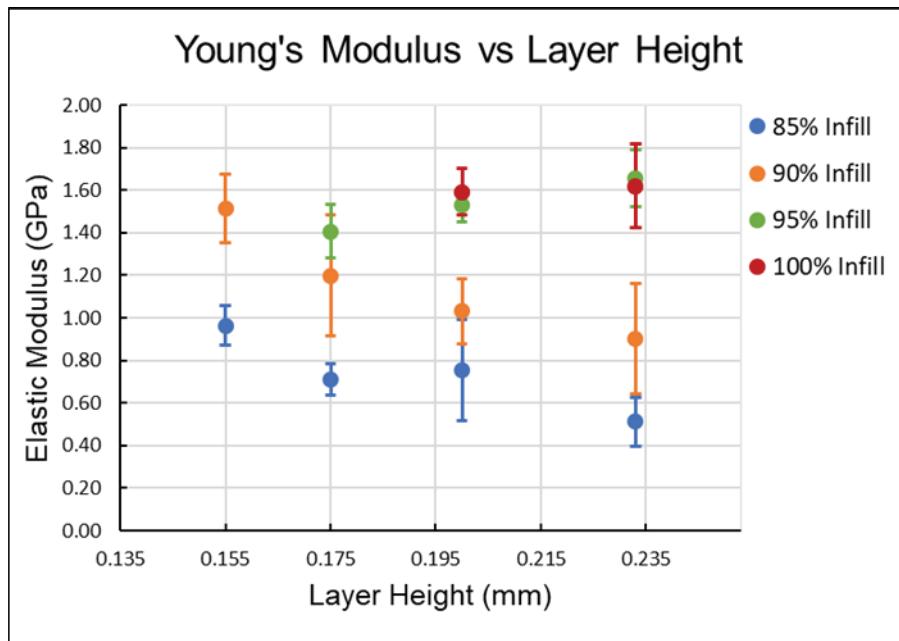**Figure 5:** The average Young's Modulus for each print, grouped by layer height.



**Figure 6:** The average Young's Modulus for each print, grouped by infill percentage.

## Ultimate Tensile Strength as a Function of Print Parameters

Similar trends were observed when comparing the UTS to print parameters. In addition to tighter groupings at higher infill percentages, Figure 7 shows a consistent, linear increase in UTS with increasing infill percentage up to a maximum of 145% improvement. Figure 8 illustrates, again, two separate trends related to layer height. While the UTS remains near-constant at 95%

and 100% infills, 85% and 90% infills demonstrate a decreasing UTS with increasing layer height – up to 31% and 34% drops, respectively.
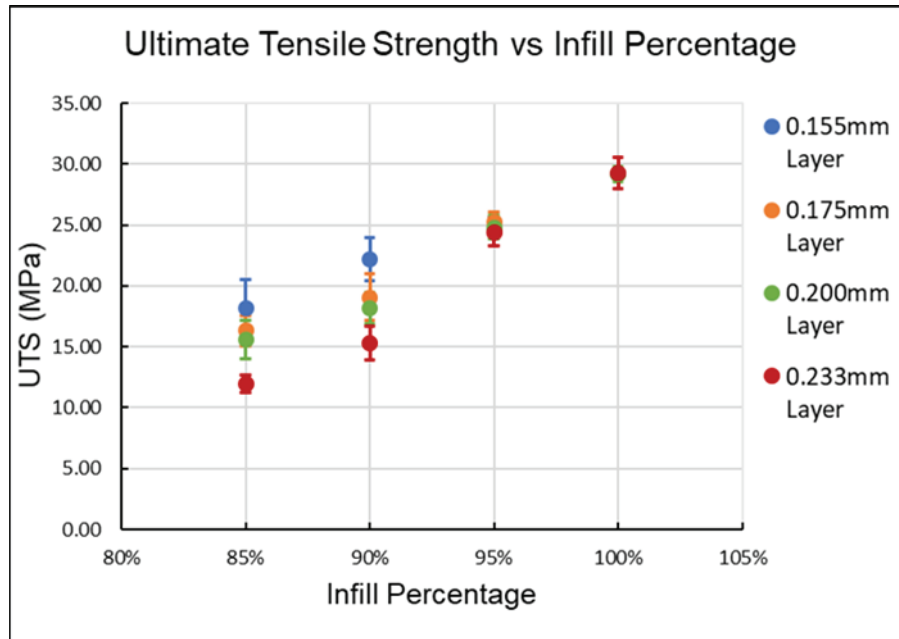


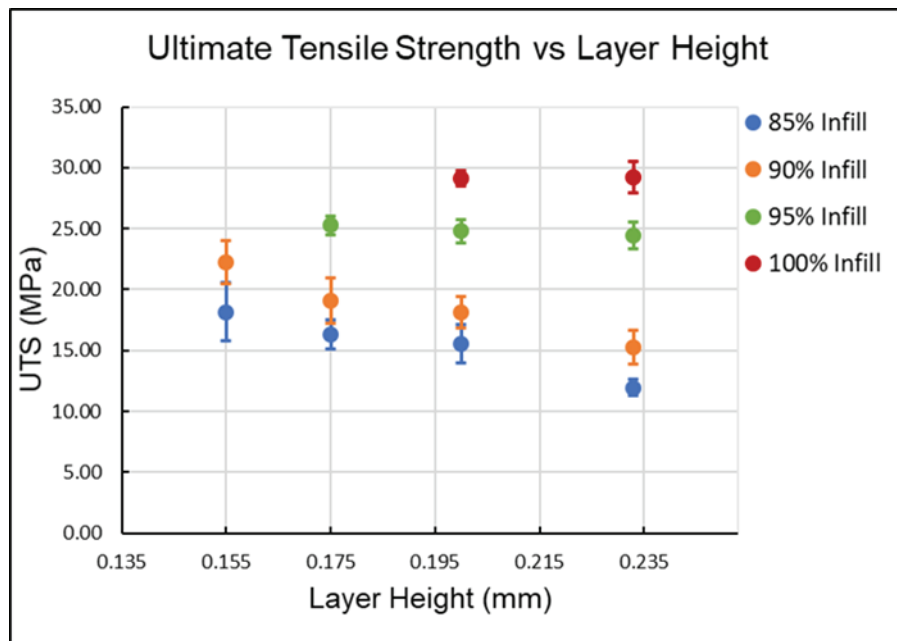**Figure 7:** The average UTS of each print, grouped by layer height.



**Figure 8:** The UTS of each print, grouped by infill percentage.

**Specific Moduli and UTS**

To complete the investigation, the mechanical properties were considered as a function of density. In Figures 9 and 10, the averages were plotted with both layer height and infill

percentage legends to establish relationships between both print parameters, porosity, and mechanical performance. For Figure 9, there is a relatively constant increase in specific modulus up to 192% at the 0.233 mm layer height at 95% infill. From here, even though the 100% infills exhibit a higher density, the lack of improvement in moduli results in a 6% decrease in specific moduli. Furthermore, a separate trend lies within each infill percentage. For the 85% and 90% infills, the specific modulus generally increases as layer height, and therefore porosity, decreases. However, for the 95% infill, the trend reverses and the increase in specific modulus is caused by an increasing density related to increasing layer height. As for the 100% infill, while there only two viable sample sets, they appear to cluster more tightly around a given value regardless of layer height. While similar trends are evident in Figure 10, they are not as distinct. Within both the 85% and 90% infill, specific UTS increases with decreasing porosity, but the 90% infill actually exhibits a lower specific UTS compared to the 85% infill. This is a result of significant densification in the 90% specimens without substantial UTS improvements. Both the 95% and 100% infills actually exhibit a performance improvement with decreasing layer height leading to an increased specific UTS. However, it is a result of dipping UTS measurements rather than reduced porosity increasing strength. Additionally, data points for each of the two infills is easily with standard deviations of each other, indicating reduced importance of the phenomenon.
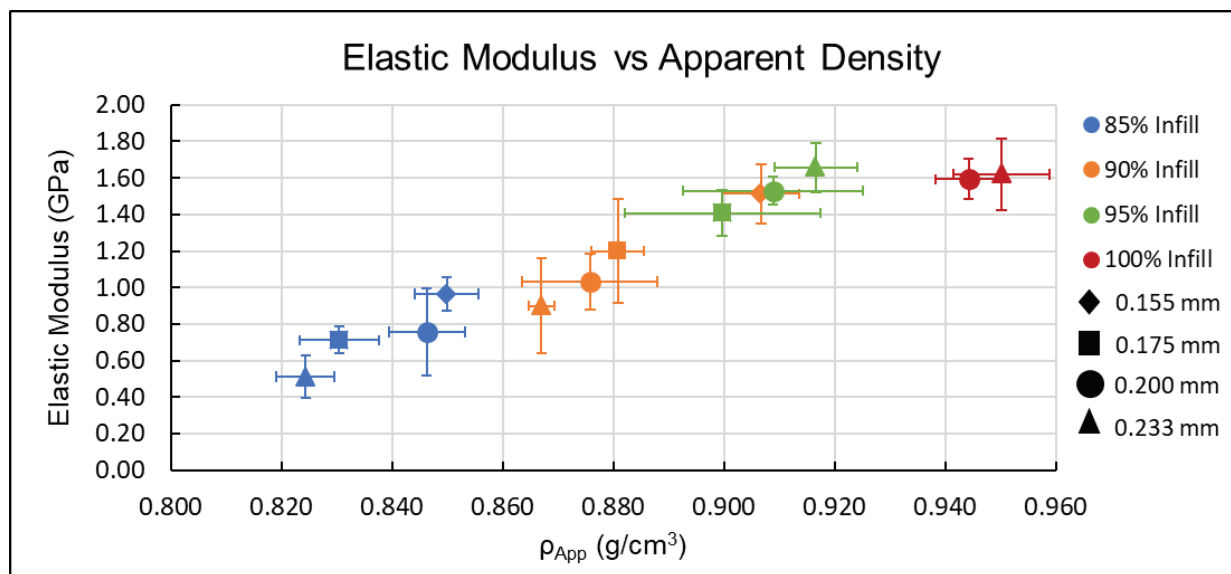


**Figure 9:** Comparison of specific moduli by plotting modulus vs density. Two legends were used, where color identifies infill percentage while shape of the point identifies the layer height.
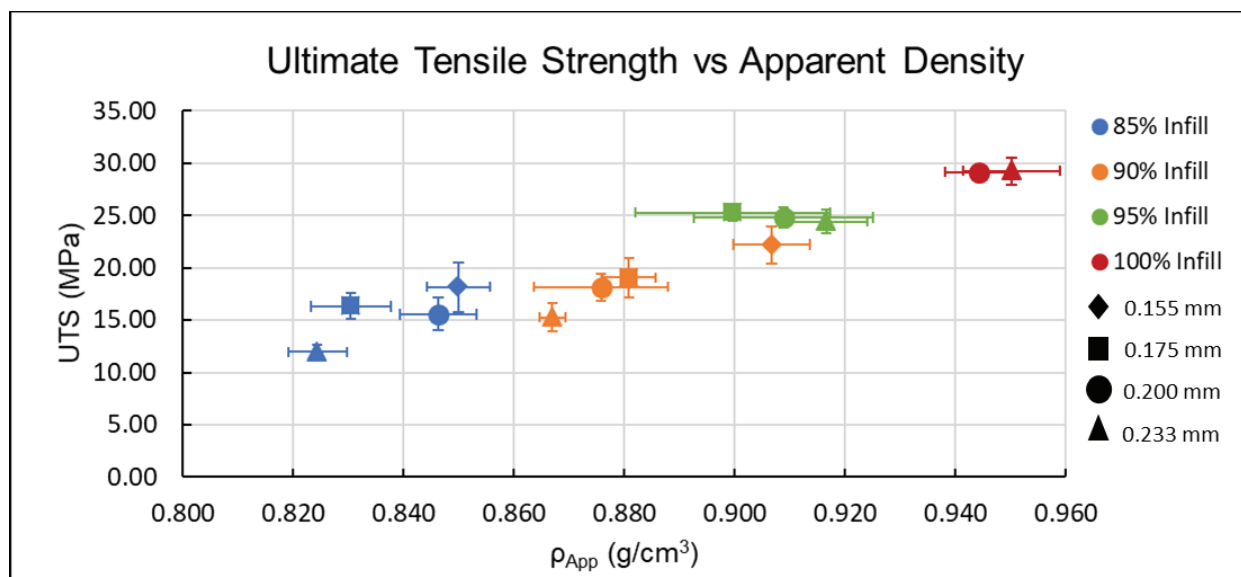
**Figure 10:** Comparison of specific UTS by plotting UTS vs density. Two legends were implemented, where color represents infill percentage while shape identifies layer height.

## Conclusions and Future Work

The vast majority of porosity in printed parts is, as expected, seen to be open celled, as shown by comparing non-inclusive density measurements for the base filament and printed parts. The densest specimens exhibited 7% porosity compared to the filament used to print them. The most porous structures were approximately 19% porous, which demonstrates a 64% reduction in porosity from the most porous print parameter pair to the densest. Considering the significant porosity in all samples, simple measurements of mechanical performance using a filament's base density are likely inaccurate and potentially misleading. As such, reporting porosity is critical to any analysis involving the effects of print parameters on mechanical properties.

Increasing the infill density of a printed part reliably increases the density, elastic modulus, and UTS of it, although the elastic modulus does not benefit from increasing the infill percentage past 95%. Similarly, at high infill percentages, increasing the layer height of a print reliably produced an increase in density, modulus, and UTS. However, at the 85% and 90% infill settings, increasing the layer height increased the porosity of the print and hampered mechanical performance. Specific moduli and UTS demonstrated unique trends in that layer height controlled the mechanical performance at a given infill percentage. Ultimately, it indicates a direct influence of the print parameters on the mechanical properties of a part while also highlighting the influence of the porosity created by the parameters' interactions.

## Acknowledgements

# References

[1]     B. Wendel, D. Rietzel, F. Kuhnlein, R. Feulner, G. Hulder, and E. Schmachtenberg, "Additive Processing of Polymers," *Macromolecular Materials and Engineering,* vol. 293, pp. 799-809, 2008 2008.

[2]     S. C. Ligon, R. Liska, J. Stampfl, M. Gurr, and R. Mulhaupt, "Polymers for 3D Printing and Customized Additive Manufacturing," (in English), *Chem. Rev.,* Review vol. 117, no. 15, pp. 10212-10290, Aug 2017, doi: 10.1021/acs.chemrev.7b00074.

[3]     E.-K. Karahaliou and P. A. Tarantili, "Preparation of poly(acrylonitrile–butadiene–styrene)/montmorillonite nanocomposites and degradation studies during extrusion reprocessing," *Journal of Applied Polymer Science,* vol. 113, no. 4, pp. 2271-2281, 2009, doi: 10.1002/app.30158.

[4]     Q. Sun, G. M. Rizvi, C. T. Bellehumeur, and P. Gu, "Effect of processing conditions on the bonding quality of FDM polymer filaments," (in English), *Rapid Prototyping J,* vol. 14, no. 2, pp. 72-80, 2008, doi: 10.1108/13552540810862028.

[5]     B. Wittbrodt and J. M. Pearce, "The effects of PLA color on material properties of 3-D printed components," *Additive Manufacturing,* vol. 8, pp. 110-116, 2015/10/01/ 2015, doi: https://doi.org/10.1016/j.addma.2015.09.006.

[6]     N. G. Tanikella, B. Wittbrodt, and J. M. Pearce, "Tensile strength of commercial polymer materials for fused filament fabrication 3D printing," *Additive Manufacturing,* vol. 15, pp. 40-47, 2017/05/01/ 2017, doi: https://doi.org/10.1016/j.addma.2017.03.005.

[7]     T. Letcher, B. Rankouhi, and S. Javadpour, *Experimental Study of Mechanical Properties of Additively Manufactured ABS Plastic as a Function of Layer Parameters*. 2015.

[8]     W. Wu, P. Geng, G. Li, D. Zhao, H. Zhang, and j. Zhao, "Influence of Layer Thickness and Raster Angle on the Mechanical Properties of 3D-Printed PEEK and a Comparative Mechanical Study between PEEK and ABS," *Materials,* vol. 8, no. 9, pp. 5834-5846, 09/01 2015, doi: 10.3390/ma8095271.

[9]     B. Rankouhi, S. Javadpour, F. Delfanian, and T. Letcher, "Failure Analysis and Mechanical Characterization of 3D Printed ABS With Respect to Layer Thickness and Orientation," *Journal of Failure Analysis and Prevention,* journal article vol. 16, no. 3, pp. 467-481, June 01 2016, doi: 10.1007/s11668-016-0113-2.

[10]    B. Huang and S. Singamneni, "Raster angle mechanics in fused deposition modelling," (in English), *J Compos Mater,* Article vol. 49, no. 3, pp. 363-383, Feb 2015, doi: 10.1177/0021998313519153.

[11]    K. Alvarez, R. Lagos, and M. Aizpun, "Investigating the influence of infill percentage on the mechanical properties of fused deposition modelled ABS parts," *Ingeniería e Investigación,* vol. 36, pp. 110-116, 12/19 2016, doi: 10.15446/ing.investig.v36n3.56610.

[12]    M. S. Hossain, D. Espalin, J. Ramos, M. Perez, and R. Wicker, "Improved Mechanical Properties of Fused Deposition Modeling-Manufactured Parts Through Build Parameter Modifications," (in English), *J Manuf Sci E-T Asme,* vol. 136, no. 6, Dec 2014, doi: Artn 06100210.1115/1.4028538.

[13]    F. Ning, W. Cong, Y. Hu, and H. Wang, "Additive manufacturing of carbon fiber-reinforced plastic composites using fused deposition modeling: Effects of process parameters on tensile properties," *J Compos Mater,* vol. 51, no. 4, pp. 451-462, 2017/02/01 2017, doi: 10.1177/0021998316646169.

[14]    S. B. Balani, F. Chabert, V. Nassiet, and A. Cantarel, "Influence of printing parameters on the stability of deposited beads in fused filament fabrication of poly(lactic) acid," *Additive Manufacturing,* vol. 25, pp. 112-121, 2019/01/01/ 2019, doi: https://doi.org/10.1016/j.addma.2018.10.012.

[15]     M. P. Serdeczny, R. Comminal, D. B. Pedersen, and J. Spangenberg, "Experimental validation of a numerical model for the strand shape in material extrusion additive manufacturing," *Additive Manufacturing,* vol. 24, pp. 145-153, 2018/12/01/ 2018, doi: https://doi.org/10.1016/j.addma.2018.09.022.

[16]     MatterHackers, "Purple MH Build Series ABS Filament - 1.75mm (1kg)," Website. [Online]. Available: https://www.matterhackers.com/store/3d-printer-filament/175mm-abs-filament-purple-1-kg.

[17]     "ASTM D638-14, Standard Test Method for Tensile Properties of Plastics," *ASTM International, West Conshohocken, PA,* 2014, doi: 10.1520/D0638-14.